Cellular and Molecular Biology
E-ISSN : 1165-158X / P-ISSN : 0145-5680
www.cellmolbiol.org

Effect of Magnetic Nanoparticles on Hormone Level Changes During Perimenopausal Period and Regulation of Bone Metabolism

Wengong Wei, Meiling Cai, Shanshan Yu, Hailin Chen, Yi Luo, Xiaoping Zhang*
Department of Obstetrics and Gynecology, Qingpu Branch, Zhongshan Hospital, Fudan University, Shanghai 201700, China

ARTICLE INFO

Original paper

Article history:
Received: July 29, 2022
Accepted: November 12, 2022
Published: December 31, 2022

Keywords:

Perimenopausal period, superparamagnetic Fe_3O_4 nanoparticle, nerve magnetic stimulation, bone metabolism, estrogen

ABSTRACT

This work aimed to explore the effect of nerve magnetic stimulation based on superparamagnetic Fe_3O_4 nanoparticle (NP) on bone metabolism during the perimenopausal period. First, the multifunctional water-soluble polymer PTMP-PMAA was utilized as the ligand. PTMP-MAA@ Fe_3O_4 NP with high magnetization was prepared by the co-precipitation method, and NPX diffraction pattern analysis and in vitro stability analysis were implemented. Then, NPs were co-cultured with 293T cells, and the cytotoxicity was detected by the CCK-8 method. Subsequently, 3-month-old female young SD rats and 11~15-month-old natural menopausal SD rats were taken as the research objects. According to the vaginal smear, the rats were randomly rolled into a young control, perimenopausal period model, estrogen treatment, and osteoporosis prevention groups. Rats in the estrogen treatment group were given Premarin suspension by gavage. Rats in the osteoporosis prevention group were injected stereotaxically with PTMP-MAA@ Fe_3O_4 NP suspension, and a rotating magnetic field was applied to the brain for nerve magnetic stimulation. The rats were sacrificed three days after treatment and brain tissues were taken for pathological analysis. Rat humerus was weighted and dual-energy X-ray was utilized to determine bone density and bone mineral content. Serum was collected and radioimmunoassay and ELISA were employed to detect estradiol (E2), osteocalcin (Boneglaprotein, BGP), oxytocin (OT), bone alkaline phosphatase (BALP), type I collagen carboxy-terminated cross-linked peptide (CTX-I), and tartrate-resistant acid phosphatase (TRACP-5b) in the serum of rats in each group. The results showed that PTMP-MAA@ Fe_3O_4 NP had good biocompatibility, and the CCK-8 test results showed that PTMP-MAA@ Fe_3O_4 NP had low cytotoxicity. Compared with the young control group, the humeral dry weight, wet weight, bone density, and bone mineral content, serum E2, OT, and BGP content in the perimenopausal period model group were reduced, while the serum BALP, CTX-I, and TRACP -5b content was increased (P<0.05). It was verified that nerve magnetic stimulation based on PTMP-MAA@ Fe_3O_4 NP increased the serum estrogen level of female rats during the perimenopausal period, increased the bone density of rats, promoted bone formation, and regulated bone metabolism.

Doi: http://dx.doi.org/10.14715/cmb/2022.68.12.17 Copyright: © 2022 by the C.M.B. Association. All rights reserved.

Introduction

The perimenopausal period refers to the period when a woman transitions from a reproductive age to an age without reproductive capacity. During the perimenopausal period, due to the changes in the levels of sex hormones in the body, the multiple metabolic processes in the body are out of balance, resulting in clinical symptoms including mental and physical symptoms. Due to changes in bone metabolism, osteoporosis will occur (1). Therefore, osteoporosis is one of the most common perimenopausal period syndromes, patients often show limb pain, difficulty in movement, etc., and severe fractures may occur (2). Modern medicine believed that the cause of osteoporosis was closely related to the changes in estrogen, thyroid hormone, and calcitonin content (3). At present, the main clinical treatment for osteoporosis in the perimenopausal period is hormone replacement. However, the risks and side effects of long-term adoption of hormone therapy have not been well resolved, which limits its clinical adoption.

Magnetic stimulation is a non-invasive method, which can directly stimulate the cerebral cortex and has a low impact on the intermediate tissues (4). Therefore, different magnetic stimulation techniques have also been widely adopted in the treatment of neurological processes and neuropsychiatric diseases. In recent years, superparamagnetic NPs, such as Fe_3O_4, have attracted widespread attention. In the absence of an external magnetic field, superparamagnetic NPs can gather together due to their unique magnetic properties. Therefore, it has the potential to achieve functions such as in vivo targeting and disease treatment (5,6). Studies showed that intravenous injection of superparamagnetic iron oxide nanomedicine can replenish a large amount of iron, and has lower adverse reactions (7). In addition, magnetic NP can also act as an enhancer for nuclear magnetic resonance imaging research, as well as in the field of neuromagnetic stimulation (8).

However, there are relatively few studies on the effects of superparamagnetic NP-based neuromagnetic stimulation on hormone levels and bone metabolism-related substances in the perimenopausal period model. Therefore, a rat model of the perimenopausal period was prepared in this work, and a superparamagnetic Fe_3O_4 NP for nerve magnetic stimulation was constructed. Subsequently,

* Corresponding author. Email: hongdouzhui47172@163.com

the estrogen treatment group was deemed as the control, and the effect of nerve magnetic stimulation on the bone metabolism of rats during the perimenopausal period was compared and analyzed. It intended to lay the foundation for the promotion of superparamagnetic NP-based neuromagnetic stimulation in the treatment of clinical diseases and improve the clinical efficacy of osteoporosis during the perimenopausal period.

Materials and Methods

Preparation of superparamagnetic Fe_3O_4 NPs

First, 5g 58mmol/L monomer pentaerythritol-4-3-mercaptopropionic acid (PTMP, 99%) and 0.56g 1.16mmol/L methacrylic acid (MAA) were dissolved in 25mL of absolute ethanol. Then, after mixing, a magnetic stirrer was employed, and the water-soluble polymer ligand PTMP-MAA was synthesized by free radical polymerization. 50 mL of deionized water was added to a three-necked flask, and nitrogen was added for 30 minutes under magnetic stirring and heat. When the temperature rose to 80°C, the polymer ligand PTMP-MAA was added to form a polymer aqueous solution (pH=4, 0.072 mM). Heating was continued, when the temperature rose to 100°C, 0.54 mmol/L $FeCl_3 \cdot 6H_2O$ and 0.27 mmol/L $FeSO_4 \cdot 7H_2O$ were dissolved in 1mL concentrated hydrochloric acid, and 15mL ammonia was immediately added. When the temperature rose to 100°C again, they were reacted for 2h. Stop heating, the solution was cooled down to room temperature under anaerobic conditions. Then, the mixed solution was added to 8000~14000 kDa dialysis bag for dialysis treatment. After 3 days, it was treated by rotary steaming at 45°C and dried in a vacuum drying oven at 45°C for 2 days to obtain PTMP-MAA@ Fe_3O_4 NPs.

Structure characterization test of superparamagnetic Fe_3O_4 NPs

A transmission electron microscope (Olympus, Japan) was employed to observe the size and morphology of PTMP-MAA@ Fe_3O_4 NPs. A dynamic light scattering instrument (Malvern, UK) was employed to detect the hydrated particle size of PTMP-MAA@ Fe_3O_4 NPs. X-ray diffractometer (Malvern Panaco, The Netherlands) was utilized to analyze the NP X-ray diffraction pattern, and the angle was set in the range of 20 to 90° to analyze the NP crystal structure.

Stability test of superparamagnetic Fe_3O_4 NPs

The dynamic light scattering instrument (Malvern, UK) was used to observe and detect the hydrated particle size of PTMP-MAA@ Fe_3O_4 NPs dissolved in aqueous solution at different time points (0h, 1h, 3h, 6h, 12h, 24h, 48h, and 168h). Then, the hydrated particle size of PTMP-MAA@ Fe_3O_4 NPs dissolved in aqueous solutions of different pH (3, 5, 7, 9, and 11) were measured and observed.

In vitro cytotoxicity test of superparamagnetic Fe_3O_4 NPs

293T cells were taken as the research object, which was cultured in high glucose DMEM medium containing 10% fetal bovine serum and 1% double-antibody. The cells were inoculated in a 96-well plate and the cell number was 8×10^3 cells per well. After cells were cultured for 24 hours in a 37°C cell incubator containing 5% CO_2, the original medium was replaced with configured DMEM medium containing different concentrations (0μg/mL, 5μg/mL, 10μg/mL, 25μg/mL, 50μg/mL, 100μg/mL, 250μg/mL, and 500μg/mL) PTMP-MAA@ Fe_3O_4 NP solution, and the culture was continued. Then, the original cell culture medium was discarded after 24h and 48h. After the cells were washed twice with phosphate buffer, 100μL of pure medium containing 10% CCK-8 reagent was added to each well. After incubation for 2h, a microplate reader (Thermo Fisher, USA) was employed to detect the absorbance of each well at 450nm. Then, the cell survival rate was calculated to analyze the cytotoxic effect of PTMP-MAA@ Fe_3O_4 NPs.

Test animals and breeding conditions

Sixty SD female rats of natural menopausal clean grade between 11 and 15 months old and 20 young female SD rats between 4 and 6 months old were selected as the research objects. Before the experiment, the rats were placed in the laboratory to adapt to the environment for 7 days. The experimental environment temperature was controlled at 20-25°C, and the relative humidity was controlled at 45-55%. Frame cage feeding standard was followed, rats were under 12h/12h day and night alternating, and free drinking water was allowed.

Preparation of perimenopausal period animal model

Natural menopausal test rats aged 11 to 15 months were adaptively fed for 7 days. On the 8th day, the smear examination of rat vaginal exfoliated cells was carried out, and the examination was continued for 10 days (2 estrus periods). The examination results of vaginal exfoliated cells in rats were evaluated according to the results shown in Table 1, and the process of estrus was evaluated. Finally, the rats with typical irregular estrus cycles (prolonged pre-estrus, no obvious pre-estrus or interval, etc.) were selected as the perimenopausal period animal model.

Test grouping and administration treatment

The 60 perimenopausal period rat models and 20 young rats were randomly rolled into the following groups. I, young control group (YC): n=20, young SD rats without any treatment were selected, and fed normally. II. perimenopausal period model group (MC): n=20, perimenopausal period SD rats without any treatment were selected, and fed normally. III, estrogen treatment group (ET): n=20, 00.0135mg/mL Premarin suspension was used, and the SD rats were intragastrically treated according to

Table 1. Picture manifestations of vaginal exfoliated cells in rats during estrus.

Estrus	Time (h)	Smear appearance of vaginal exfoliated cell
Pre-estrus	17~21	A large number of nuclear cells, only a few keratinocytes, no white blood cells.
Estrus	9~15	A lot of keratinocytes, a few nucleated cells.
Post-estrus	10~14	Large numbers of keratinocytes and white blood cells.
Estrus interval	60~70	A large number of white blood cells, small amounts of epithelial cells and mucus.

the 0.2mL/100g body weight per perimenopausal period, once a day, for 4 weeks. IV, osteoporosis prevention group (OP): n=20, the PTMP-MAA@ Fe_3O_4 NPs prepared previously were diluted to a concentration of 2.45mg/mL. After intraperitoneal injection of 10% chloral hydrate for the perimenopausal period SD rat model, the rats were fixed to the stereotactic frame, the skull was drilled and the brain tissue was exposed. 200nL PTMP-MAA@ Fe_3O_4 nanosuspension was slowly and microinjected into the paraventricular nucleus of the hypothalamus of rats at the speed of 0.05μL/min. After the injection, the head of the rats was sutured and disinfected, and the rats were put back into the cage for normal feeding when they woke up. Seven days after stereotactic injection, the rats were fixed and placed in a magnetic field for external magnetic field intervention. The minimum magnetic field intensity was set at 50mT, which was applied twice a day for 1h each time for 8w.

Histopathological examination

Three days after treatment, the rats in each group were anesthetized by intraperitoneal injection of 10% chloral hydrate, and the rats were killed. The brain tissue was fixed and made into paraffin sections with a thickness of 4μm. After dewaxing treatment, hematoxylin dye was used for dyeing for 5min, and then sections were rinsed with tap water. The tissues were differentiated with hydrochloric acid ethanol solution for 30s and soaked in tap water for 15min. Eosin staining was performed for 2min, and then sections were rinsed with tap water. After the routine dehydration treatment, the tissue was transparent and sealed. The histopathological morphology of the rat brain was observed using a light microscope (Olympus, Japan).

Bone density and bone mineral content detection

Three days after treatment, the rats in each group were anesthetized by intraperitoneal injection of 10% chloral hydrate, and the rats were killed. The left femur of rats was taken and the muscle and fascia were removed. The bone weight was weighed before and after drying and the data were recorded. The femur was placed under a measuring instrument, and the bone mineral density and bone mineral content of rats in each group were detected by the dual-energy X-ray measuring instrument.

Serological index detection

Three days after treatment, the rats in each group were anesthetized by intraperitoneal injection of 10% chloral hydrate, and the rats were killed. Serum samples were collected from each group, estradiol (E2) and osteocalcin (BGP) were detected by radioimmunoassay. Then, in accordance with the ELISA kit instructions, detection of the concentration of rat serum oxytocin (OT), BALP, CTX-I, and TRACP 5b was performed. First, the standard product was diluted and then the standard curve was drawn. After the serum sample to be tested was added, it was incubated at a constant temperature with the antibody. After washing, color developing agent was added for incubation, then washing. After the termination solution was added, the absorbance was measured at 450nm using an enzyme-plate analyzer (Bio-Rad, USA). The concentrations of OCN, BALP, CTX-I, and TRACP-5b were finally calculated.

Statistical analysis

Mean ± standard deviation ($\bar{x}\pm s$) was how measurement data were expressed. SPSS19.0 was employed for data analysis. One-way ANOVA analysis of variance was used for pair comparison between groups, and $P<0.05$ was considered to be statistically significant.

Results and Discussion

Structural characterization of superparamagnetic Fe_3O_4 NPs

Superparamagnetic NPs referred to NPs with a magnetic response, in which Fe_3O_4 and Fe2O3 were the most important parts of magnetic nanomaterials (9). In this work, the multifunctional superparamagnetic NPs were prepared, and the characterization and analysis of PTMP-MAA@Fe_3O_4NP were performed. From Figure 1A, the particle size of the prepared PTMP-MAA@Fe_3O_4 hydrated NP was about 40nm, and the NP sub-sizes were uniform and the distribution was relatively dispersed. The particle size distribution was then tested. From Figure 1B, the particle size distribution of PTMP-MAA@Fe_3O_4 NP was in the range of 20~70nm, and the average particle size was 37.9±10.8nm. To determine the crystal structure of the prepared PTMP-MAA@Fe_3O_4 NP, X-ray diffraction (XRD) analysis was performed. From Figure 1C, the diffraction peaks of PTMP-MAA@Fe_3O_4 NP had an excellent crystal structure, and specific diffraction peaks appeared at 23.1°, 29.3°, 37.6°, 47.7°, 53.5° and 59.1°. Such results were in line with the spinel structure characteristics of magnetic Fe_3O_4 NP (10).

In vitro stability analysis of superparamagnetic Fe_3O_4 NPs

Since the internal environment of biological organisms is very complicated, it is necessary to analyze the stability of NPs in vitro before they were applied in vivo (11). PTMP-MAA@Fe_3O_4 NPs were dissolved in an aqueous solution, and the change of hydrated particle size at different time points was detected. From Figure 2A, the hydrated particle size of the PTMP-MAA@Fe_3O_4 NP prepared

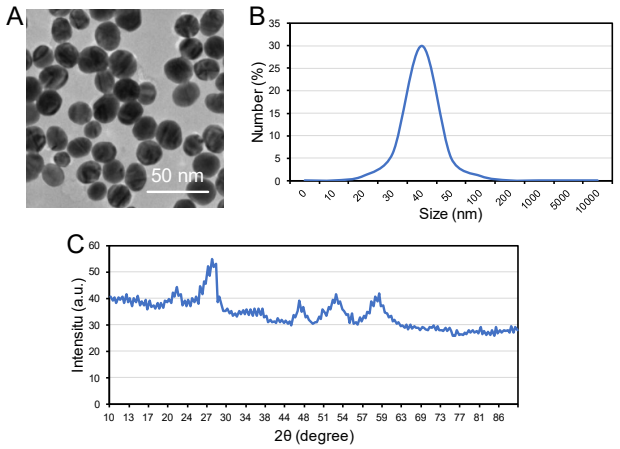

Figure 1. Structure characterization results of superparamagnetic Fe_3O_4 NP. (A) Transmission electron micrograph of PTMP-MAA@ Fe_3O_4 NP. (B) Hydration particle size distribution of PTMP-MAA@ Fe_3O_4 NP. (C) XRD pattern of PTMP-MAA@ Fe_3O_4 NP.

fluctuated in the range of 35-50nm at different time points. Moreover, the solution was always clear, and there was no agglomeration of NPs. Since the acidity and alkalinity levels inside the organism are not the same, the changes of PTMP-MAA@Fe_3O_4 NP hydrated particle size was also tested under different pH aqueous solutions. From Figure 2B, the hydrated particle size of the PTMP-MAA@Fe_3O_4 NP prepared in different pH aqueous solutions fluctuated in the range of 35~45nm. The particle size in the neutral aqueous solution was not much different. The above results showed that PTMP-MAA@Fe_3O_4 NP had good time stability and pH stability characteristics, and can be used in subsequent in vivo tests.

Cytotoxicity analysis of superparamagnetic Fe_3O_4 NPs

Since magnetic NP has the characteristics of magnetic guidance, low cytotoxicity, and good biocompatibility, it has been widely used in the biomedical field (12,13). To further verify the biocompatibility characteristics of PTMP-MAA@Fe_3O_4 NP, the CCK-8 method was used to detect the effect of different concentrations of PTMP-MAA@Fe_3O_4 NP on the viability of 293T cells, so as to evaluate the cytotoxicity of PTMP-MAA@Fe_3O_4 NP. The results were presented in Figure 3, with the increase of PTMP-MAA@Fe_3O_4 NP concentration, the activity of 293T cells after 24h and 48h culture was always higher than 90%, suggesting that the PTMP-MAA@Fe_3O_4 NP prepared in this work had good biocompatibility and low cytotoxicity, and can be used in subsequent in vivo tests.

Morphological and pathological examination results of rat brain tissue in each group

PTMP-MAA@ Fe_3O_4 NP was stereotactic injected into the paraventricular nucleus of the hypothalamus of rats, and the pathological changes of the brain were observed after neuromagnetic stimulation. Brain tissues of rats in each group were collected and pathological sections of HE staining were made. From Figure 4, the number and density of neuron cells in each group were moderately distributed, and the nucleoli could be clearly seen. The nucleolus showed basophilic characteristics while the cytoplasm showed acidophilic characteristics. No significant pathological changes were observed in the brain tissue of each group. Therefore, it was considered safe to inject PTMP-MAA@ Fe_3O_4 NP suspension into rats.

Test results of humerus weight and strength in each group of rats

The differences of the wet weight and dry weight of the humerus in each group were compared. From Figure 5A and Figure 5B, compared with the YC group, the wet and dry weights of the humerus in the MC group were significantly reduced, and the difference was considerable (P<0.05). However, the wet weight and dry weight of the humerus in the YC group were not obviously different from those in the ET and OP groups (P>0.05). Compared with the rats in the MC group, the wet weight and dry weight of the humerus in the ET group and OP group increased notably, with substantial differences (P<0.05).

The differences between the humeral bone mineral density (BMD) and bone mineral content (BMC) of each

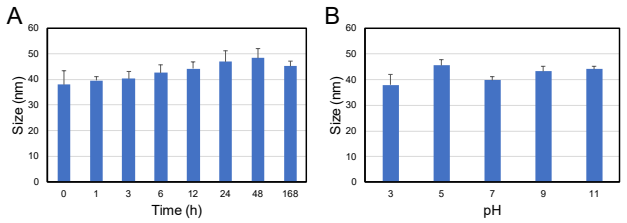

Figure 2. In vitro stability test results of superparamagnetic Fe_3O_4 NP. (A) PTMP-MAA@ Fe_3O_4 NP hydrated particle size changes in neutral aqueous solutions at different time points. (B) PTMP-MAA@ Fe_3O_4 NP hydrated particle size changes in aqueous solutions with different pH.

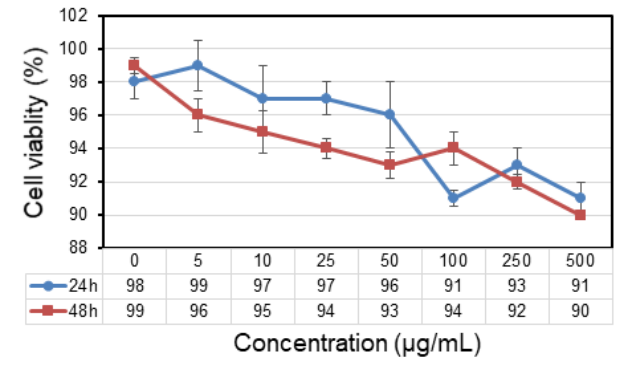

Figure 3. Cytotoxicity test results of superparamagnetic Fe_3O_4 NP.

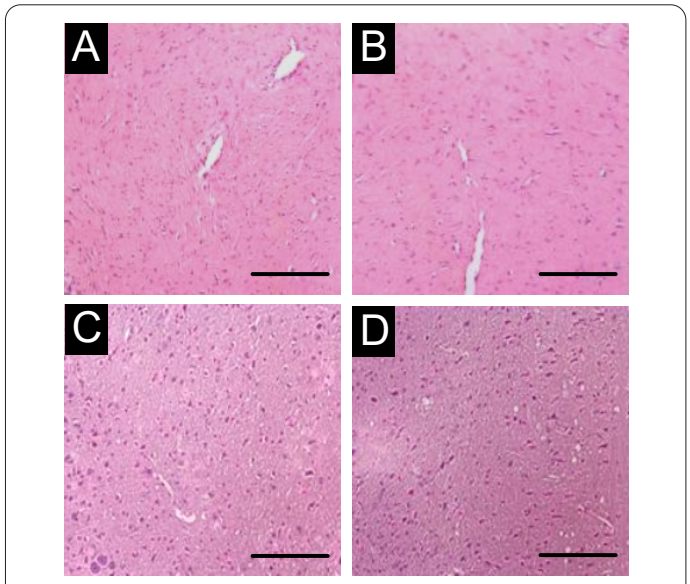

Figure 4. HE staining results of rat brain tissue sections (400×, bar=25μm). (A) HE staining of rat brain slices in the YC group. (B) HE staining of rat brain slices in the MC group. (C) HE staining of rat brain slices in the ET group. (D) HE staining of rat brain slices in OP group.

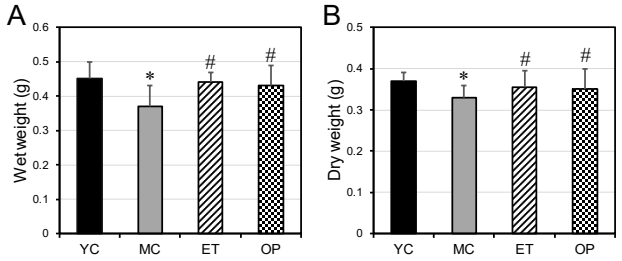

Figure 5. Comparison of the wet and dry weight of rat humerus. (A) Comparison of the wet weight of humerus. (B) Comparison of the dry weight of humerus. Compared with the YC group, *P<0.05; Compared with the MC group, #P<0.05.

group of rats were compared. From Figure 6A and Figure 6B, compared to the YC group, the BMD and BMC of the humerus of rats in the MC group were significantly reduced, and the difference was remarkable (P<0.05). However, the BMD and BMC of the humerus of the YC group were not greatly different from those of the ET and OP groups (P>0.05). Compared with the rats in the MC group, the BMD and BMC of the humerus of the rats in the ET group and the OP group increased considerably, and the difference was obvious (P<0.05).

Serological index test results of rats in each group

The differences in the levels of estradiol (E2) and oxytocin (OT) in the serum of rats in each group were compared. From Figure 7A and Figure 7B, compared with the YC group, the serum E2 and OT contents of the MC group were greatly reduced, with substantial differences (P<0.05). However, the serum E2 and OT contents of YC group were not obviously different from those of ET group and OP group (P>0.05). Compared with the rats in the MC group, the serum E2 and OT levels in the ET group and the OP group increased remarkably (P<0.05). OT is a kind of post-pituitary hormone. Studies suggested that it can directly regulate bone metabolism. When OT levels increase, it can stimulate bone cell differentiation and bone formation (14). It was found in this work that the serum OT level of rats in the ET group and the OP group increased, indicating that the neuromagnetic stimulation based on superparamagnetic NP can promote the differentiation and bone formation of rat bone cells during the perimenopausal period.

The differences in serum concentrations of osteocalcin (BGP), bone alkaline phosphatase (BALP), type I collagen carboxy-terminal cross-linking peptide (CTX-I), and anti-tartrate acid phosphatase (TRACP-5b) were compared. From Figure 8A, Figure 8C, and Figure 8D, compared with the YC group, the serum BGP, CTX-I, and TRACP-5b levels of rats in the MC group were notably increased, and the difference was considerable (P<0.05). However, the levels of serum BGP, CTX-I, and TRACP-5b in the YC group were not substantially different from those in the ET and OP groups (P>0.05). In contrast to the rats in the MC group, the serum BGP, CTX-I, and TRACP-5b levels in the ET group and the OP group were obviously reduced, with a remarkable difference (P<0.05). From Figure 8B, compared with the YC group, the serum BALP content of rats in the MC group was substantially reduced (P<0.05). However, there was no great difference in serum BALP content between YC group and ET group and OP group (P>0.05). Compared with the rats in the MC group, the levels of serum BALP in the ET group and the OP group increased evidently, and the difference was remarkable (P<0.05).

BGP, BALP, and CTX-I are biochemical indicators commonly used to assess bone formation, and TRACP-5b is a marker used to assess bone resorption (15-17). It was found that nerve magnetic stimulation based on superparamagnetic NP can reduce the levels of BGP, CTX-I, and TRACP-5b, and can increase the level of BALP, indicating that nerve magnetic stimulation based on superparamagnetic NP can balance the bone formation and bone resorption state of rats during the perimenopausal period.

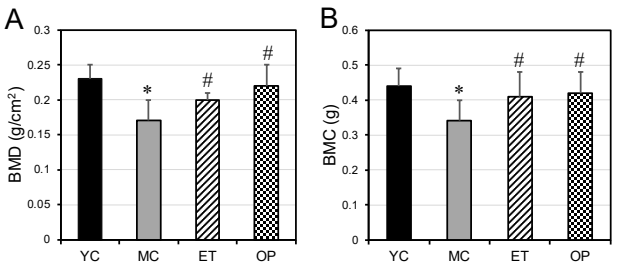

Figure 6. Comparison of bone mineral density and bone mineral content of humerus in rats. (A) Comparison of humeral bone density. (B) Comparison of humeral bone mineral content. Compared with the YC group, *P<0.05; Compared with the MC group, #P<0.05.

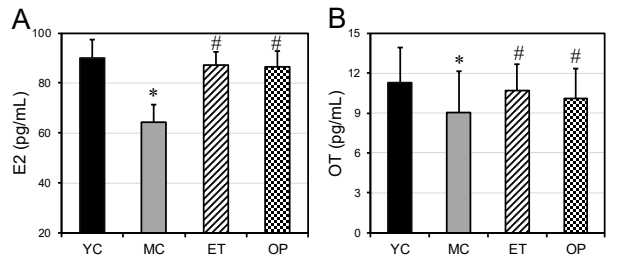

Figure 7. Comparison of serum estradiol and oxytocin levels in rats. (A) Comparison of serum estradiol. (B) Comparison of serum oxytocin. Compared with the YC group, *P<0.05; Compared with the MC group, #P<0.05.

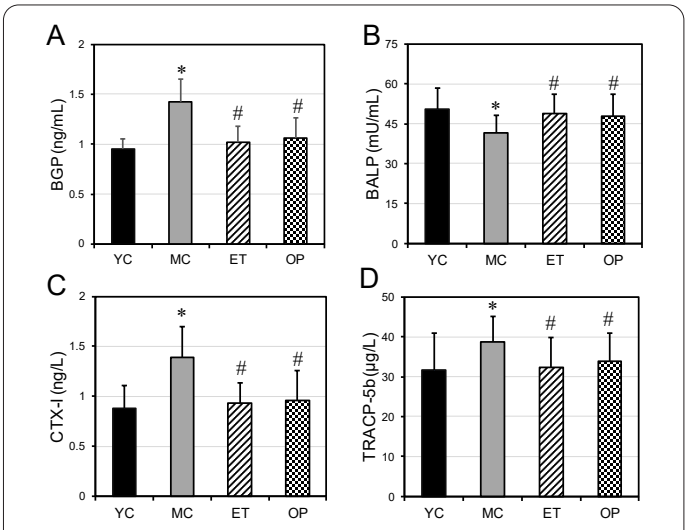

Figure 8. Comparison of rat serum osteocalcin, bone alkaline phosphatase, type I collagen carboxy-terminated cross-linked peptide, and tartrate-resistant acid phosphatase. (A) Comparison of serum osteocalcin. (B) Comparison of bone alkaline phosphatase. (C) Comparison of type I collagen carboxy-terminated cross-linked peptide. (D) Comparison of tartrate-resistant acid phosphatase. Compared with the YC group, *P<0.05; Compared with the MC group, #P<0.05.

Conclusion

In this work, the superparamagnetic Fe_3O_4 NPs for nerve magnetic stimulation were prepared first. After analysis, it was found that the NPs prepared had low cytotoxicity and excellent biocompatibility characteristics. Then, the rat model of the perimenopausal period was constructed. The adoption of superparamagnetic Fe_3O_4 NP-based neural magnetic stimulation can significantly increase the serum estrogen level in rats. In addition, it can also regulate the bone metabolism process of rats in the perimenopausal period, balances the bone formation and bone resorption state of rats, and then improves the osteoporosis

of rats in the perimenopausal period. However, this work only explores the effect of nerve magnetic stimulation based on superparamagnetic Fe_3O_4 NP on serum hormone levels in rats during the perimenopausal period. In the future, the sample size needs to be expanded to explore the specific regulation mechanism. In conclusion, the results can provide a basis for the promotion of neuromagnetic stimulation in the clinical treatment of diseases and the improvement of the symptoms of osteoporosis during the perimenopausal period.

Fundings

The research is supported by: Characteristic project of health system in Qingpu District (No. WX2019-03).

References

1. Willi J, Ehlert U. Assessment of perimenopausal depression: A review. J Affect Disord. 2019 Apr 15;249:216-222. doi: 10.1016/j.jad.2019.02.029. Epub 2019 Feb 11. PMID: 30776662.
2. Marjoribanks J, Farquhar C, Roberts H, Lethaby A, Lee J. Long-term hormone therapy for perimenopausal and postmenopausal women. Cochrane Database Syst Rev. 2017 Jan 17;1(1):CD004143. doi: 10.1002/14651858.CD004143.pub5. PMID: 28093732; PMCID: PMC6465148.
3. Miller PD. Management of severe osteoporosis. Expert Opin Pharmacother. 2016;17(4):473-88. doi: 10.1517/14656566.2016.1124856. Epub 2015 Dec 23. PMID: 26605922.
4. Geng Yuehua, Xing Yangyang, Zhang Xin, Ge Manling. Complexity analysis of EEG under magnetic stimulation on acupoint of Guangming(GB37). Annu Int Conf IEEE Eng Med Biol Soc. 2017 Jul;2017:2316-2319. doi: 10.1109/EMBC.2017.8037319. PMID: 29060361.
5. He Z, Chen Z, Tan M, Elingarami S, Liu Y, Li T, Deng Y, He N, Li S, Fu J, Li W. A review on methods for diagnosis of breast cancer cells and tissues. Cell Prolif. 2020 Jul;53(7):e12822. doi: 10.1111/cpr.12822. Epub 2020 Jun 12. PMID: 32530560; PMCID: PMC7377933.
6. Yang G, Xiao Z, Tang C, Deng Y, Huang H, He Z. Recent advances in biosensor for detection of lung cancer biomarkers. Biosens Bioelectron. 2019 Sep 15;141:111416. doi: 10.1016/j.bios.2019.111416. Epub 2019 Jun 6. PMID: 31279179.
7. Liu L, Hitchens TK, Ye Q, Wu Y, Barbe B, Prior DE, Li WF, Yeh FC, Foley LM, Bain DJ, Ho C. Decreased reticuloendothelial system clearance and increased blood half-life and immune cell labeling for nano- and micron-sized superparamagnetic iron-oxide particles upon pre-treatment with Intralipid. Biochim Biophys Acta. 2013 Jun;1830(6):3447-53. doi: 10.1016/j.bbagen.2013.01.021. Epub 2013 Feb 8. PMID: 23396002; PMCID: PMC3640706.
8. Wang C, Huang Y, Zhu H, Wang Z, Chen Z, Chen H, Li S, He N, Liu T. Design and Implementation of High-Throughput Magnetic Separation Module for Automated Nucleic Acid Detection System Based on Magnetic Nano-Beads. J Nanosci Nanotechnol. 2020 Apr 1;20(4):2138-2143. doi: 10.1166/jnn.2020.17327. PMID: 31492222.
9. Li L, Zhong D, Xu Y, Zhong N. A novel superparamagnetic micro-nano-bio-adsorbent PDA/Fe_3O_4/BC for removal of hexavalent chromium ions from simulated and electroplating wastewater. Environ Sci Pollut Res Int. 2019 Aug;26(23):23981-23993. doi: 10.1007/s11356-019-05674-1. Epub 2019 Jun 20. PMID: 31222649.
10. Lu H, Zhang L, Ma J, Alam N, Zhou X, Ni Y. Nano-Cellulose/MOF Derived Carbon Doped CuO/Fe_3O_4 Nanocomposite as High Efficient Catalyst for Organic Pollutant Remedy. Nanomaterials (Basel). 2019 Feb 16;9(2):277. doi: 10.3390/nano9020277. PMID: 30781506; PMCID: PMC6410010.
11. Zheng X, Chen Y, Wang Z, Song L, Zhang Y, Gu N, Xiong F. Preparation and *In Vitro* Cellular Uptake Assessment of Multifunctional Rubik-Like Magnetic Nano-Assemblies. J Nanosci Nanotechnol. 2019 Jun 1;19(6):3301-3309. doi: 10.1166/jnn.2019.16129. PMID: 30744757.
12. Chen H, Wu Y, Fang Y, Liao P, Zhao K, Deng Y, He N. Integrated and automated, sample-in to result-out, system for nanotechnology-based detection of infectious pathogens. Nanosci Nanotechnol Lett 2018 Oct 1;10(10):1423-8.
13. He Z, Tang C, Chen X, Liu H, Yang G, Xiao Z, Li W, Deng Y, Jin L, Chen H, Chen Z. Based on magnetic beads to develop the kit for extraction of high-quality cell-free DNA from blood of breast cancer patients. Materials Express. 2019 Nov 1;9(8):956-61.
14. Colaianni G, Tamma R, Di Benedetto A, Yuen T, Sun L, Zaidi M, Zallone A. The oxytocin-bone axis. J Neuroendocrinol. 2014 Feb;26(2):53-7. doi: 10.1111/jne.12120. PMID: 24219627; PMCID: PMC4108483.
15. Song YE, Tan H, Liu KJ, Zhang YZ, Liu Y, Lu CR, Yu DL, Tu J, Cui CY. Effect of fluoride exposure on bone metabolism indicators ALP, BALP, and BGP. Environ Health Prev Med. 2011 May;16(3):158-63. doi: 10.1007/s12199-010-0181-y. Epub 2010 Oct 2. PMID: 21431799; PMCID: PMC3078298.
16. Alavi, M., Hamblin, M. Antibacterial silver nanoparticles: effects on bacterial nucleic acids. Cell Mol Biomed Rep 2023; 3(1): 35-40. doi: 10.55705/cmbr.2022.361677.1065.
17. Eick GN, Devlin MJ, Cepon-Robins TJ, Kowal P, Sugiyama LS, Snodgrass JJ. A dried blood spot-based method to measure levels of tartrate-resistant acid phosphatase 5b (TRACP-5b), a marker of bone resorption. Am J Hum Biol. 2019 May;31(3):e23240. doi: 10.1002/ajhb.23240. Epub 2019 Mar 21. PMID: 30897260.